

Exploring clogging of interacting particles with hydrodynamic memory in a corrugated channel: A promising sensor of non-Brownian diffusion

Yuhui Luo(罗玉辉), Chunhua Zeng(曾春华), and Tao Huang(黄韬)

Citation: Chin. Phys. B, 2025, 34 (**8**): 080508. DOI: 10.1088/1674-1056/adecfc
http://cpb.iphy.ac.cn; http://iopscience.iop.org/cpb

What follows is a list of articles you may be interested in

Distributed dynamic event-based finite-time dissipative synchronization control for semi-Markov switched fuzzy cyber-physical systems against random packet losses

Xiru Wu(伍锡如), Yuchong Zhang(张煜翀), Tiantian Zhang(张畑畑), and Binlei Zhang(张斌磊)
Chin. Phys. B, 2023, 32 (**10**): 100506. DOI: 10.1088/1674-1056/acb91b

Robust H_∞ state estimation for a class of complex networks with dynamic event-triggered scheme against hybrid attacks

Yahan Deng(邓雅瀚), Zhongkai Mo(莫中凯), and Hongqian Lu(陆宏谦)
Chin. Phys. B, 2022, 31 (**2**): 020503. DOI: 10.1088/1674-1056/ac0ee9

Ratchet transport of overdamped particles in superimposed driven lattices

Shu-Na Huang(黄淑娜), Wei-Jing Zhu(朱薇静), Xiao-Qun Huang(黄小群), Bao-Quan Ai(艾保全), Feng-Guo Li(李丰果)
Chin. Phys. B, 2019, 28 (**4**): 040502. DOI: 10.1088/1674-1056/28/4/040502

One-dimensional mass transport with dynamic external potentials

Xingxing Zhang(张星星), Dongqin Zheng(郑冬琴), Weirong Zhong(钟伟荣)
Chin. Phys. B, 2019, 28 (**2**): 020505. DOI: 10.1088/1674-1056/28/2/020505

Collective transport of Lennard–Jones particles through one-dimensional periodic potentials

Jian-hui He(何健辉), Jia-le Wen(温家乐), Pei-rong Chen(陈沛荣), Dong-qin Zheng(郑冬琴), Wei-rong Zhong(钟伟荣)
Chin. Phys. B, 2017, 26 (**7**): 070502. DOI: 10.1088/1674-1056/26/7/070502

SPECIAL TOPIC — A celebration of the 90th Anniversary of the Birth of Bolin Hao

Exploring clogging of interacting particles with hydrodynamic memory in a corrugated channel: A promising sensor of non-Brownian diffusion

Yuhui Luo(罗玉辉)[1], Chunhua Zeng(曾春华)[2,†], and Tao Huang(黄韬)[2]

[1] *School of Physics and Information Engineering, Zhaotong University, Zhaotong* 657000, *China*
[2] *Faculty of Science, Kunming University of Science and Technology, Kunming* 650500, *China*

(Received 9 May 2025; revised manuscript received 25 June 2025; accepted manuscript online 8 July 2025)

Particle transport is a fundamental aspect of various systems, from artificial to biological. A common assumption is that particle motion follows Markovian (memoryless) processes in the absence of interaction between particles. However, hydrodynamic memory and the interaction between particles are ubiquitous, leaving many fundamental questions unanswered regarding transport of interacting particles involving hydrodynamic drag in corrugated channels, as described by the fractional Langevin equation. This study examines the hydrodynamic transport of interacting non-Brownian particles moving within a corrugated channel. We propose a method that relies on factors such as temperature, the driving force to alternate between no transport and finite net transport. Of importance is to note that the absence of transport results from the clogging, while the transport consists of collective motion and independent motion. The transport systems investigated in this work suggest the potential for sensor functionality within the system. Our findings may prove valuable for exploring the transport with hydrodynamic memory in various fields, including biology, physics, and chemistry.

Keywords: particle transport, clogging, non-Brownian diffusion, hydrodynamic memory, sensor

PACS: 05.20.Dd, 05.10.–a, 05.40.–a, 05.30.Pr

DOI: 10.1088/1674-1056/adecfc **CSTR:** 32038.14.CPB.adecfc

1. Introduction

Transport plays a crucial role in numerous fields, including physics,[1–3] biology,[4] medicine,[5] chemistry, and materials science. Since the early 2000s, extensive research has been conducted on the transport of particles moving through various channels or tubes under diverse conditions. Examples of theoretical investigation include entropic transport,[1] entropic splitter[6] and inertial effects[7] for Brownian particle, entropic electrokinetics for ions,[8] manipulating chiral microswimmers,[9] and active Brownian motion.[10] Examples of experimental investigation include stochastic sensing with single protein pores[11] and hydrodynamic and entropic effects for colloidal particles.[12] These transports are frequently studied in molecular sieves, nano- and micro-pores, ion channels, chromatography, and membrane channels.[13] Moreover, they also have a key role in particle separation and bioparticle focusing applications in clinical diagnostics.[14] Most works mentioned above studied the transport of noninteracting particles with Stokes memoryless friction. Therefore, the transport with Stokes memoryless friction in channels or tubes has been thoroughly understood. However, for the random walker interacting with its environment, memory effects cannot be neglected.[15] The transport with a hydrodynamic memory for particles moving in a corrugated channel remains to be elucidated.

It is well-known that the transports for experimental study in channels or tubes were extensively investigated in numerous fields, such as the traffic of a viral motor channel for double-stranded DNA translocation,[4] a viral DNA-packaging motor channel in lipid bilayers,[16] myeloid cell migration in vascular channels,[17] Piezo2 channel promoting cell mechanobiological responses,[18] a calcium-permeable channel triggering plant immune signaling,[19] mechanically activated ion channels,[20] the platelet SOC channel leading to pathological thrombus formation.[5] One important question is what factors affect the transport or escape of particles in a channel? Previous theoretical and experimental investigations demonstrated that the volume of the confining domain and the starting point to aperture distance greatly affect narrow escape time of the particles.[21] Moreover, aperture size also influences escape rates in microbial narrow escape.[22] Motility parameters of active particles impact the narrow-escape time from circular domains.[23] A natural question is how the temperature affects the transport with hydrodynamic memory in a corrugated channel? Do these factors result in the occurrence of the clogging?

Transport with a hydrodynamic memory for theoretical investigation has been extensively studied in various sys-

†Corresponding author. E-mail: zchh2009@126.com

© 2025 Chinese Physical Society and IOP Publishing Ltd. All rights, including for text and data mining, AI training, and similar technologies, are reserved.

tems. Examples for a hydrodynamic drag include fractional Brownian motors,[24] the transport optimization in rocking ratchets,[25] nonlinear transport,[26] anomalous transport,[27] anomalous kinetics of magnetosensitive ion channels,[28] etc. Additionally, the transport of fractional Brownian motion has also been investigated in several systems, such as transport and escape in a deformable channel.[29] It should be noted that a dynamical equation involving hydrodynamic memory can correspond to a fractional differential equation, which may potentially encompass a fractional Langevin equation.[30–33] Systems characterized by fractional differential equations have been extensively investigated in various fields since the early 2000s, such as fractional cable models,[34] Chua's circuit model with fractional order,[35] a financial system with fractional calculus,[36] fractional Josephson effect,[37] fractional Schrödinger equation.[38] However, studying systems with hydrodynamic memory is challenging due to the complexity of fractional dynamical equations. Anomalous phenomena have been identified in such systems, which are characterized by fractional differential equations.

In recent decades, significant interest has been devoted to the transport of particles moving within corrugated channels or tubes. However, previous explorations have primarily focused on the transport of noninteracting particles.[1,6,8] In reality, interactions among particles in various systems are ubiquitous and, in some cases, cannot be overlooked. Consequently, numerous studies over the past 20 years have examined the interactions between particles in a wide range of settings. Examples include repulsive power-law interactions,[39] nonlinear interactions,[40] hydrodynamic interactions,[41] long range interactions,[42] time-dependent interactions,[43] etc. This raises the question of whether the interaction causes the jamming or clogging, which leads to the disappearance of the transport. It should be noted that both jamming and clogging[44–46] resulting from interaction have been extensively investigated in the last decades in various systems. Examples of experiment investigation include granular hopper flows,[44] the jamming of soft disks,[46] and jamming transition in granular systems.[47] The general case for the transport of interacting particles with hydrodynamic memory moving in corrugated channels or tubes remains open. It should be noted that a widespread assumption for interacting particles is the Lennard–Jones potential.[12] Besides transport with hydrodynamic drag, other anomalous phenomena with hydrodynamic memory in corrugated channels or tubes are also of great interest. Examples include the hydrodynamic memory leading to hyperdiffusion,[31] resonances,[32] and superdiffusion.[33] Moreover, fractional Brownian motion has also been studied in many works, such as nonergodicity and heterogeneous diffusion,[48] and transient aging.[49] However, to our best knowledge, the transport of interacting particles with hydrodynamic memory remains unexplored in a corrugated channel.

2. Model and methods

We here consider interacting particles with memory kernel and non-Brownian diffusion moving in a corrugated channel which is characterized by a fractional friction coefficient and fractional Gaussian noise.[24–26,32,50] Thus the particle evolves as

$$m_k\ddot{\boldsymbol{r}}_k + \int_0^t \boldsymbol{\eta}_k(t-t')\dot{\boldsymbol{r}}_k\,\mathrm{d}t' = \boldsymbol{F} + \boldsymbol{F}_{\mathrm{int}} + \boldsymbol{\xi}_k(t), \tag{1}$$

where $k = 1,2,\ldots,N$, N is the number of interacting particles. m_k is the mass of the kth particles. $\boldsymbol{r}_k(t) = (x_k(t), y_k(t))^{\mathrm{T}}$ denotes the position of the kth particle at time t. $\boldsymbol{F} = (F,0)^{\mathrm{T}}$ and $\boldsymbol{F}_{\mathrm{int}} = -\nabla U_{\mathrm{int}}(\boldsymbol{r})$ denote the driving force and the interaction forces between particles. Here $U_{\mathrm{int}}(\boldsymbol{r})$ is the Lennard–Jones potential and given by $U_{\mathrm{int}}(\boldsymbol{r}) = 4\epsilon[(\frac{\sigma}{\boldsymbol{r}})^{12} - (\frac{\sigma}{\boldsymbol{r}})^{6}]$, where ϵ and σ are the coupling strength and characteristic length of the Lennard–Jones potential, respectively. $\boldsymbol{\xi}_k(t)$ is a Gaussian noise and its statistical properties are as follows:

$$\langle \xi_{ki}(t)\rangle = 0, \quad \langle \xi_{ki}(t)\xi_{kj}(t')\rangle = k_{\mathrm{B}}T\delta_{i,j}\eta_k(|t-t'|),$$

where $i,j = x,y$, and $\boldsymbol{\eta}_k(t)$ is the memory kernel. For the two-dimensional structure depicted in Fig. 1, we consider a reflection symmetric sinusoidally shaped channel as follows:

$$w_{\pm}(x) = \pm 0.25\Big[(g_{\mathrm{w}} + g_{\mathrm{n}}) - (g_{\mathrm{w}} - g_{\mathrm{n}})\cos(2\pi x)\Big],$$

where the parameters g_{n} and g_{w} represent its minimum (called the bottleneck) and maximum width, respectively.

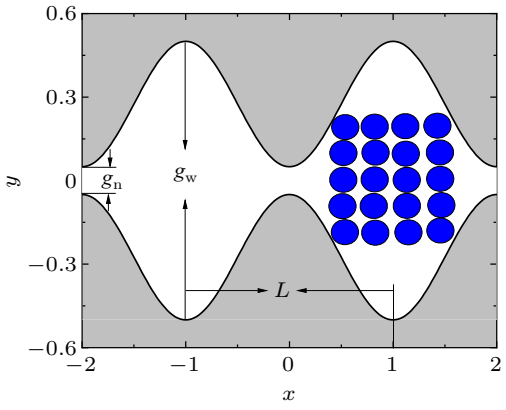


Fig. 1. A segment of the corrugated channel confining the underdamped motion of interacting particles with non-Brownian diffusion. L and g_{n} are the periodicity and the the bottleneck, respectively. The radii of particles (blue spheres) are equal to $\sigma/2$. The parameters are $g_{\mathrm{w}} = 1.0$, $g_{\mathrm{n}} = 0.1$, $\sigma = 0.05$, and $L = 2.0$.

Through the fractional Riemann–Liouville derivative, the frictional term can be recast. Equation (1) is rewritten as follows:[50]

$$m_k\ddot{\boldsymbol{r}}_k + \eta_\alpha\, {}_0\hat{D}_t^{\alpha-1}\dot{\boldsymbol{r}}_k = \boldsymbol{F} + \boldsymbol{F}_{\mathrm{int}} + \boldsymbol{\xi}_k(t), \tag{2}$$

where α is the power-law exponent of diffusion without the interaction, boundaries, and driving forces, ${}_0\hat{D}_t^{\alpha-1}$ is the

Riemann–Liouville fractional derivative. To realize numerical simulation of Eq. (2), we introduce auxiliary variables M and the corresponding multi-dimensional Markovian dynamics $\boldsymbol{u}_i$ as follows:

$$\begin{aligned}
&\frac{\mathrm{d}\boldsymbol{r}_k(t)}{\mathrm{d}t} = \boldsymbol{v}_k(t),\\
&m\frac{\mathrm{d}\boldsymbol{v}_k(t)}{\mathrm{d}t} = \boldsymbol{F} + \boldsymbol{F}_{\mathrm{int}}\\
&\qquad\qquad - \sum_{i=1}^{M} \boldsymbol{u}_{ki}(t) - \eta_0 \boldsymbol{v}_k(t) + \sqrt{2k_{\mathrm{B}}T\eta_0}\boldsymbol{\xi}_{k0}(t),\\
&\frac{\mathrm{d}\boldsymbol{u}_{ki}(t)}{\mathrm{d}t} = -\eta_i \boldsymbol{v}_k(t) + \mu_i \boldsymbol{u}_{ki}(t) + \sqrt{2k_{\mathrm{B}}T\eta_i\mu_i}\boldsymbol{\xi}_{ki}(t). \quad (3)
\end{aligned}$$

Here $\boldsymbol{v}_k(t) = (v_{kx}(t), v_{ky}(t))^{\mathrm{T}}$, $\boldsymbol{u}_k(t) = (u_{kx}(t), u_{ky}(t))^{\mathrm{T}}$, $\mu_i = \mu_0/b^i$, $\eta_i = C_\alpha(b)\eta_\alpha\mu_i^\alpha/|\Gamma(1-\alpha)|$ for $i = 1, 2, \ldots, M$ (i denotes the ith auxiliary variable), and $\eta_0 = \sum_{i=1}^{M}\eta_i/\mu_i = 6\pi\rho_{\mathrm{f}}\mu R$ (Stokes friction coefficient). Here ρ_{f}, μ, and R are the liquid density, kinematic viscosity, and radius of particles with mass density ρ. $\boldsymbol{\xi}_{k0}(t)$ and $\boldsymbol{\xi}_{ki}(t)$ are Gaussian white noises with mean zero and variance one. $\boldsymbol{\xi}_{k0}(t)$ is given by

$$\boldsymbol{\xi}_{k0}(t) = \sum_{i=1}^{M}\sqrt{\frac{\eta_i}{\mu_i\eta_0}}\boldsymbol{\xi}_{ki}(t).$$

We fix $\alpha = 3/2$, $m = 1.0$, and $g_{\mathrm{w}} = 1.0$, unless otherwise stated. All quantities are in dimensionless units. Based on Ref. [50], we here take $\mu_0 = 1000$ and $b = 5$. According to $\langle\Delta\boldsymbol{r}^2(t)\rangle = \langle\boldsymbol{r}^2(t)\rangle - \langle\boldsymbol{r}(t)\rangle^2 \propto t^\alpha$, we here choose auxiliary particles M to guarantee $\alpha = 3/2$ in diffusion without interaction, the driving force, and the limitation of the corrugated channel. We present the diffusion in Fig. A1 of Appendix A, which shows that for $M = 13$, α is equal to $3/2$.

The Fokker–Planck equation corresponding to the generalized Langevin equation (1) is generally unsolvable. As a result, the transport and corresponding statistical properties of interacting particles moving within the system are investigated through numerical simulations. We employ the stochastic Euler algorithm[50] with time step $\Delta t = 10^{-4}$ to discretize Eq. (3).

To characterize the anomalous transports and their statistical properties, we first analyze the dynamical behaviors of the system through the average velocity and diffusion. We analyze these results through the phase-space map. For initial conditions, the positions of all particles are arranged in a grid pattern at a period. The initial positions $x_k(0)$ and $y_k(0)$ range from $L/3$ to $2L/3$ and from $-0.7g_{\mathrm{w}}$ to $0.7g_{\mathrm{w}}$, respectively. The auxiliary variables $u_{kx}(0)$ follow a Gaussian distribution with zero mean and variance $LT\eta_i$ in intervals $[0, L]$, while $u_{ky}(0)$ follow a Gaussian distribution with zero mean and variance $T\eta_i$. Due to a result depending on the initial conditions, the average velocity calculations incorporate 50 realizations with different initial conditions. To interpret the findings depending on the initial conditions, we present this result in Fig. A2 in Appendix A. We thus test the other scheme whose results are identical to these results. Namely, the initial positions $x_k(0)$ and $y_k(0)$ are uniformly distributed over the intervals $[-L/2, L/2]$ and $[-0.1w(x), +0.1w(x)]$, respectively. The initial distance between two particles is larger than 0.5σ. The initial velocities $v_{kx}(0)$ and $v_{ky}(0)$ both follow a Gaussian distribution with zero mean and variance T. Moreover, the auxiliary variables $u_{kx}(0)$ follow a Gaussian distribution with zero mean and variance $LT\eta_i$ in intervals $[-L/2, L/2]$, while $u_{ky}(0)$ follow a Gaussian distribution with zero mean and variance $T\eta_i$. To achieve a convergent result, 10^7 time steps of the initial transient state are removed, and 10^8 time steps of the steady state are utilized for each trajectory. We employ an inelastic boundary condition, as described in Ref. [51]. It defines an inelastic wall at which the particle does not move at all if the step would take it into the forbidden region. Namely, for the step in the forbidden region, the position of the particle does not change and its velocity becomes zero.

3. The result

In order to examine the transport of interacting particles, we present the average velocity $\langle v\rangle$ as a function of both temperature T and driving force F in Fig. 2. It is shown that for a small F, there exists a maximum with the increase of T. For a large F, there coexist maxima and minima of $\langle v\rangle$ with the increase of T. Figure 2 also shows that the transport disappears for a high temperature. It is worth noting that these nonlinear transports happen when the bottleneck g_{n} is equal to the characteristic length σ. Furthermore, for $g_{\mathrm{n}} > \sigma$ (i.e., $g_{\mathrm{n}} = 0.3$), $\langle v\rangle$ monotonically decreases with the increase of T, as shown in Fig. A3 of Appendix A. Moreover, for a fixed T, $\langle v\rangle$ increases with the driving force F. Based on the transport resulting from the change of the temperature and driving force, we, therefore, propose that the transition between no transport and a finite net transport may realize the sensor of interacting particles with non-Brownian diffusion. The sensor is potentially useful for exploring the transports of interacting colloidal particles, microswimmers, ions, etc.

To comprehend the underlying physical mechanisms of these results, we analyze the dynamical relaxation through the time series, phase space, and probability distributions corresponding to points A–D of Fig. 2 for different time intervals. To see how temperature affects the transport, we present the time series of 20 interacting particles for the time ranging from $t = 0$ to 100 (Figs. 3(a)–3(d)) and from $t = 1000$ to 1100 (Figs. 3(e)–3(h)). For $T = 0.001$, figure 3(a) shows that for the initial state, 20 interacting particles correspond to 20 curves, whereas there exist three curves first, then two curves, and three curves finally. It should be noted that 18 interacting particles remain in the initial positions, suggesting that the clog-

ging arises, labelled by "Clogging" in Fig. 3(a). To provide more insight into the clogging, we present the corresponding phase space in Fig. 3(i), displaying that there exist two particles moving in phase space, and other 18 interacting particles remain at the initial positions and form the clogging. For the steady state, there exist three curves in Fig 3(e), showing that the clogging still appears. This implies that the average velocity is trivial due to the clogging for most of the particles and the mobility for a few particles. This finding agrees with that corresponding to point A in Fig. 2. Figure 3(b) shows that two particles move together for a long period of time, suggesting that collective motion occurs, labelled by "Collective motion". Although these behaviors corresponding to $T = 0.01$ in Fig. 3(b) are similar to those corresponding to $T = 0.001$ in Fig. 3(a), the mobility of $T = 0.01$ is smaller than that of $T = 0.001$, as shown in Fig. 3(b), 3(f), and 3(j). The reason is twofold. One is collective motion; the other is presented in Fig. 3(j), showing that as the temperature increases, the motions of particles in the y direction are larger than those in Fig. 3(i). This weakens their motions in the x direction. Namely, the distances for motions of the x direction in Fig. 3(j) are smaller than those in Fig. 3(i). Therefore, this is the reason why $\langle v \rangle$ corresponding to $T = 0.001$ is larger than that corresponding to $T = 0.01$. Figures 3(b) and 3(f) also show that there exists the clogging. It should be noted that the clogging was investigated in several systems, such as deep neural networks,[52] vertebrate body axis elongation,[53] agitated frictional granular matter.[54]

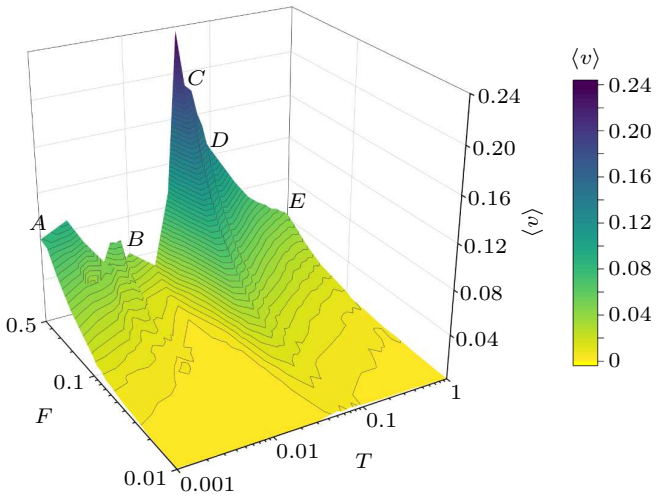


Fig. 2. The average velocity $\langle v \rangle$ as a function of temperature T and driving force F. The other parameters are $\varepsilon = 0.5$, $\sigma = 0.1$, $g_n = 0.1$, $N = 20$, and $L = 2.0$. The transports of points A–E are analysed through the time series in Fig. 3 and the probability distribution functions in Fig. 4.

For $T = 0.05$, figure 3(c) shows that most of the curves overlap at beginning and they separate each other with time evolution. This suggests that the clogging arises initially and then disappears. We present the corresponding phase space in Fig. 3(k), showing that there exist four particles moving while other 16 particles basically remain in initial positions because of the appearance of the clogging. We find that for steady state, all curves range from $x = 50$ to 250 in Fig. 3(g), suggesting that there exist two cases: one is that curves are independent, indicating the interaction between particles disappears for the steady state; the other is that the curves overlap, indicating that the interaction between particles remains, suggesting that collective motion arises. The motion in y direction corresponding to $T = 0.01$ is smaller than that corresponding to $T = 0.05$ and the distance in x direction of the former is larger than that of the latter. The corresponding interaction between particles sustains a short time, then the interaction disappears, which leads to that all particles move in the system. This means that the transport is enhanced. The rationale for this observation is that as the temperature increases, the motion of particles becomes dominated by the random force due to the competition between this random force and the interacting force. Conversely, at low temperatures, the motion is primarily governed by the interactions between particles.

At $T = 0.1$, figure 3(d) shows that the number of curves increases with time, revealing that for most particles, the interaction between particles vanishes with time evolution. We present the phase space in Fig. 3(l), showing that as the temperature continues to increase, the motion of particles is dominated by both random force and the driving force, and its mobility in the y direction becomes nontrivial. Notice that the particles corresponding to $T = 0.01$ and 0.05 trivially move in the y direction. This finding suggests that this behavior weakens the transport in the x direction due to the confinement imposed by the geometric structure. The behavior is shown in Fig. 3(h) for the steady state, displaying that the distances in the x direction are smaller than those corresponding to $T = 0.05$ in Fig. 3(g). Moreover, several curves overlap in Fig. 3(h), implying that the interaction between particles still remains in the steady state for certain particles and there exists collective motion too. Therefore, the transport occurs at $T = 0.1$ and becomes small. Moreover, figure 3(h) shows that the magnitudes of $x(t)$ for the part of particles basically remain constant with time evolution, implying that these particles basically remain in a place for a long time. Thus, the average velocity of the x direction becomes trivial or zero for most of the particles.

Based on these results, we find that at low temperature, the clogging appears due to the presence of the interaction for most particles, and the rest of the particles move independently in the system. Thus the corresponding transport of particles is trivial. The transport for most interacting particles does not occur because this clogging is similar to a solid-like state, as shown in Figs. A2(c) and A2(i). With the increase in temperature, the motion of the particles is dominated by the combination of random force and driving force. This leads to that the interaction for part of particles gradually disappears with time evolution, and the interaction for the other part of par-

ticles remains, leading to collective motion. Moreover, the motion in the y direction is trivial. These two behaviors enhance the transport of interacting particles in the x direction. Thus the directional transport arises at a suitable temperature because this behavior is similar to a liquid-like state, as shown in Figs. A2(f) and A2(l). At a high temperature, particles nontrivially move in the y direction resulting from a large random force, this weakens the transport in the x direction. Namely, the motion of particles is dominated by random force, thus the interacting and the driving forces become negligible. This phenomenon is similar to a gas-like state, which does not lead to directional transport. Therefore, the transport almost disappears at high temperatures.

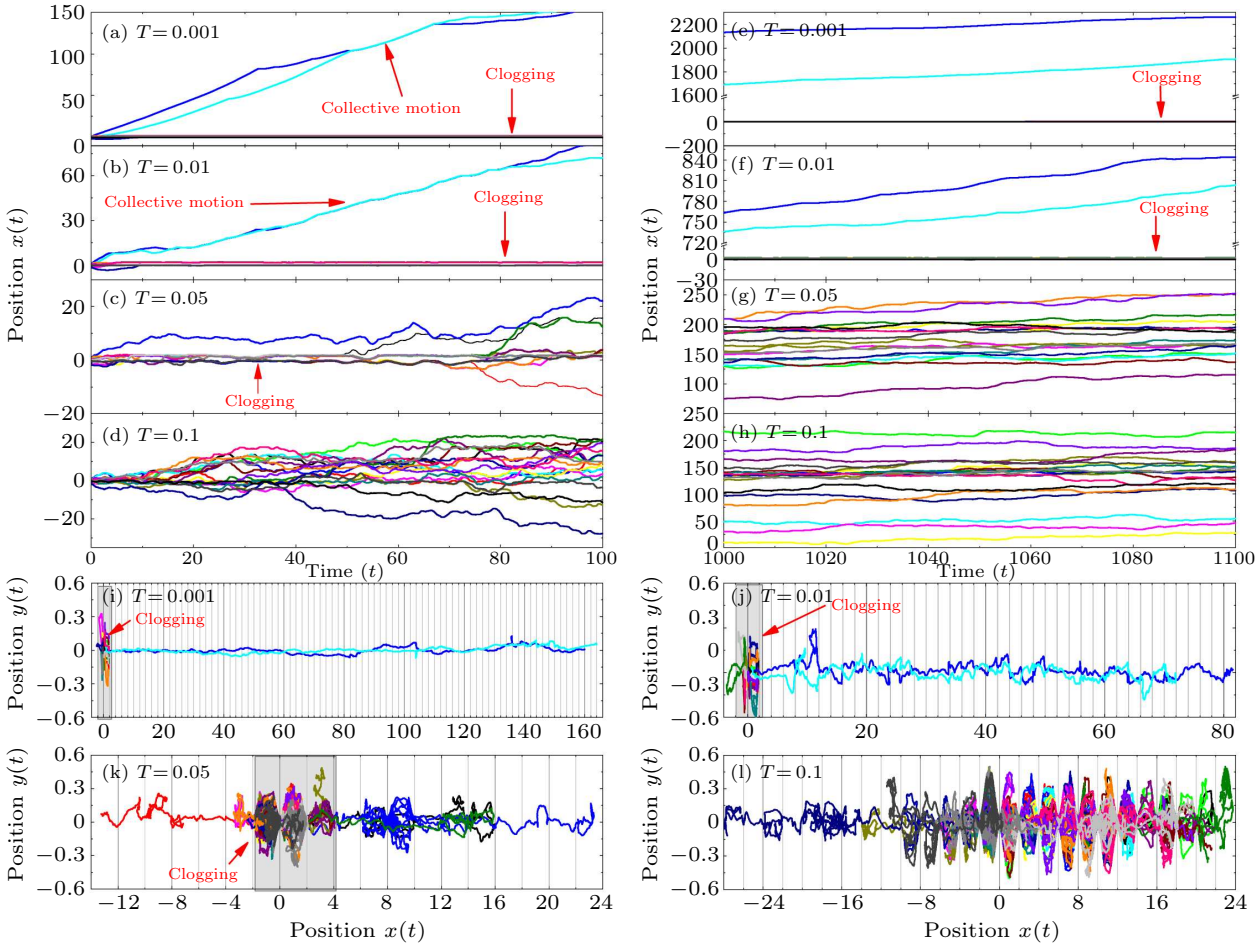


Fig. 3. The time series of $x(t)$ for interacting particles with different temperatures for the time ranging (a)–(d) from $t = 0$ to 100 and (e)–(h) from $t = 1000$ to 1100. The order number of particles is indicated by the color code. The phase spaces (i)–(l) correspond to time series (a)–(d), respectively. The other parameters are identical with those in Fig. 2. Panels (a), (e), and (i) correspond to point A; panels (b), (f), and (j) correspond to point B; panels (c), (g), and (k) correspond to point C; panels (d), (h), and (l) correspond to point D in Fig. 2.

To gain more insight into the dynamics of the system, we present the normalized probability distribution function corresponding to points A–E in Fig. 2 for a time ranging from $t = 0$ to 100 ($P_i(x)$) in Fig. 4(a) and time ranging from $t = 1000$ to 1100 ($P_s(x)$) in Fig. 4(c). For $T = 0.001$ and 0.01, figure 4(a) displays that the maximum of the normalized probability distribution locates in the initial position (the black and red curves), suggesting that the clogging appears. We also find that there exist numerous peaks in the normalized probability distribution, which correspond to the bottleneck of the corrugated channel in Fig. 4(b). The reason is that there exists the clogging in the bottleneck. The higher these peaks are, the more serious the clogging is. With the increase of the temperature (i.e., $T = 0.05$ and 0.1), the maximum of the normalized probability distribution decreases at the initial position, and the magnitudes of probability distributions increase close to the initial positions. For example, the distribution corresponding to $T = 0.1$ is larger than that corresponding to $T = 0.01$ at the place ranging from $x = 4$ to 44. Figure 4(c) shows the normalized probability distribution function of the steady state for different temperatures. At $T = 0.001$ or 0.01, most of particles are at the initial positions, indicating the appearance of the clogging, and a few particles move to far positions, e.g., $x = 300$, 700, etc. With the increase of the temperature (i.e., $T = 0.05$ and 0.1), the magnitude of probability distribution becomes small at initial positions, and the particles move a small distance in the x direction. For a high temperature (i.e., $T = 1.0$), the motion of the particles is almost dominated by

random force, and the effects of interaction and driving force are negligible. Thus the distribution is basically symmetric in the positive and negative directions of x, revealing that the transport of interacting particles disappears. This is a gas-like state. In a word, this is a consequence of the competition among interaction, driving force, temperature, and geometric structure of the system.

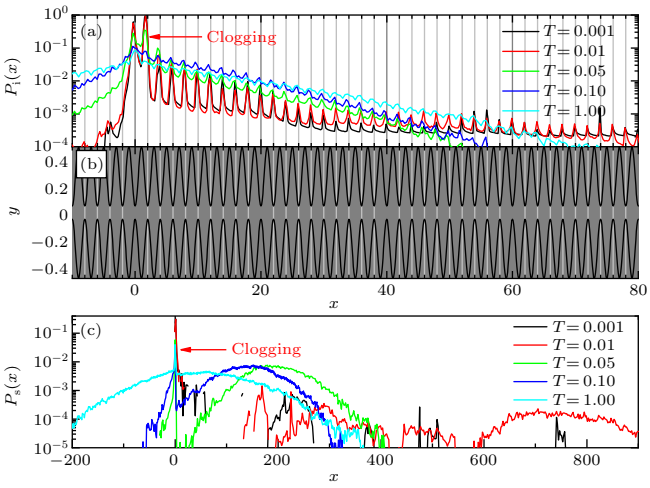


Fig. 4. The probability distribution functions of different temperatures for (a) initial transient state (time ranging from $t = 0$ to 100) and (c) steady state (time ranging from $t = 1000$ to 1100). They are obtained via 200 ensembles, each of which includes 20 interacting particles. To interpret the clogging transition, we also present the corrugated channel (b). The other parameters are identical to those of Fig. 3.

To gain a deeper understanding of the impact of the number of interacting particles on clogging, figure 5 presents the average velocity $\langle v\rangle$ as a function of the number of interacting particles N for different temperatures. It shows that for a low temperature (e.g., $T = 0.01$), the velocity dramatically decreases with the increase of N. As the temperature increases, the decrease obviously becomes trivial with the increase of N, such as $T = 0.02$. For a high temperature, the average velocity is almost constant with the increase of N, such as $T = 0.05$. In a word, the finding suggests that the clogging occurs with the increase of N.

To understand the interaction in the system, we present the average velocity $\langle v\rangle$ as a function of temperature T without and with interaction in Fig. 6. It shows that $\langle v\rangle$ decreases with the increase of T without interaction, whereas with interaction, $\langle v\rangle$ increases first and then decreases with the increase of temperature T. Namely, this outcome results from the competition between the interaction force and the random force. The random force is small at low temperatures, the interaction force governs particle motion in the competition. Conversely, the random force is large at high temperatures and dominates particle motion in this competition.

To control the occurrence of clogging, we also change the period and bottleneck of the corrugated channel. We present $\langle v\rangle$ as a function of the bottleneck g_n and the period of the system L in Fig. 7. It shows that for the bottleneck $g_n < 0.1$, $\langle v\rangle$ is trivial (i.e., $\langle v\rangle < 10^{-2}$). For $g_n > 0.1$, the transport sharply increases with g_n. Namely, the increase of the bottleneck induces the transition from no transport to a finite net transport. Why does the transport disappear for $g_n < 0.1$? The reason is that the bottleneck g_n is smaller than the characteristic length σ of the Lennard–Jones potential. This results in the appearance of the clogging, which leads to the disappearance of the transport. Moreover, with the presence of transport, $\langle v\rangle$ trivially increases with L for a fixed g_n. This suggests that a finite net transport may vanish for a trivial period. Therefore, the bottleneck and the period nontrivially affect the transport of interacting particles. This observation indicates that the clogging serves as a sensor, with its function being explored through the bottleneck and period.

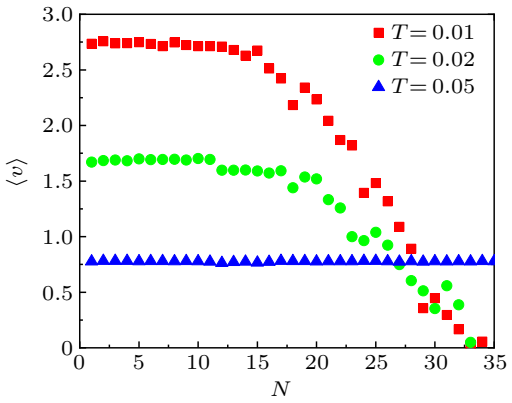


Fig. 5. The average velocity $\langle v\rangle$ as a function of the number of interacting particles. The other parameters are $F = 0.5$, $\varepsilon = 0.5$, $g_n = 0.3$, and $\sigma = 0.1$.

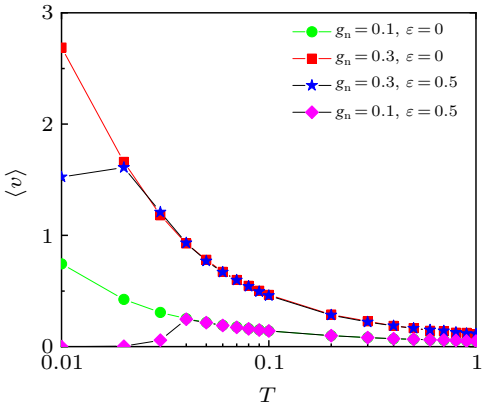


Fig. 6. The average velocity $\langle v\rangle$ as a function of temperature T without and with the interaction. The other parameters are $F = 0.5$, $N = 20$, and $\sigma = 0.1$.

Besides the change through the variation of the bottleneck and the period, we also change the characteristic length σ of the Lennard–Jones potential. Figure 8 shows the average velocity as a function of the coupling strength ε and characteristic length σ of the Lennard–Jones potential. It is shown that for a small σ, the average velocity remains unchanged with the increase in ε, e.g., $\sigma = 0.02$. This implies that for a

small σ, the coupling between interacting particles can be neglected, and the corresponding transports are similar to those of noninteracting particles. However, for a large σ, the transport basically remains unchanged first, then sharply decreases with the increase of ε (e.g., $\sigma = 0.2$). The findings suggest that the increase of σ results in the appearance of clogging and the transport disappears. Next we discuss how ε affects the transport. For a small ε (i.e., $\varepsilon = 0.2$), $\langle v \rangle$ trivially decreases with increase of σ. For a large ε (i.e., $\varepsilon = 0.5$), $\langle v \rangle$ remains unchanged first, then sharply decreases with increase of σ. This means that a large σ and a large ε give rise to the disappearance of the transport stemming from the clogging. In a word, the combination of ε and σ leads to transition between no transport and a finite net transport.

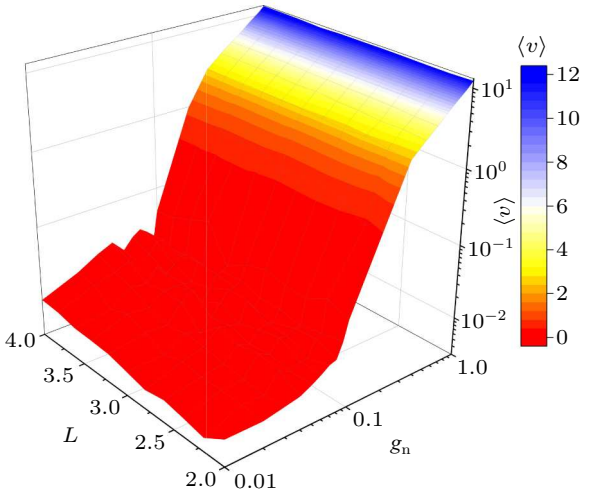


Fig. 7. The average velocity as a function of the bottleneck g_n and the periods L . The other parameters are $F = 0.5$, $N = 20$, $T = 0.01$, $\varepsilon = 0.5$, and $\sigma = 0.1$.

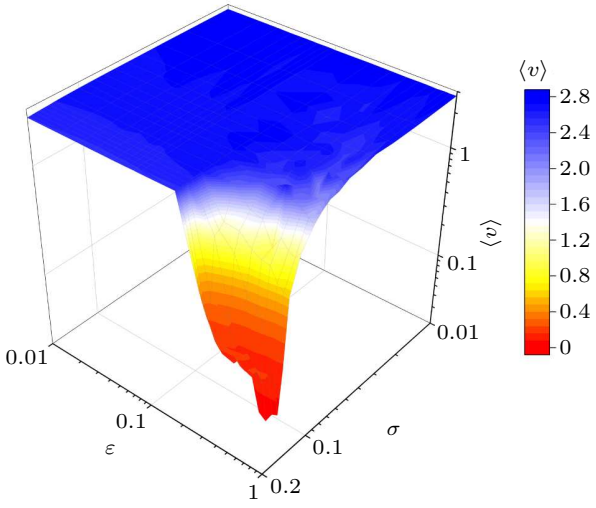


Fig. 8. The average velocity as a function of the coupling strength ε and characteristic length σ of the Lennard–Jones potential. The other parameters are $F = 0.5$, $T = 0.01$, $N = 20$, $g_n = 0.3$, and $L = 2.0$.

4. Discussion and conclusion

In order to address the questions posed in the introduction, we explore the hydrodynamic transport of interacting particles with non-Brownian diffusion in a corrugated channel. By numerical simulation of a fractional stochastic differential equation, we present how the geometric structure of the channel, interaction, temperature and driving force switch between no transport and a finite net transport in the system. These findings can be summarized as follows: An increase in driving force promotes a transition from no transport to a finite net transport within the system, whereas a rise in temperature triggers a transition from a finite net transport back to no transport. Additionally, increasing the number of interacting particles results in the occurrence of clogging. Without interactions, transport decreases monotonically with temperature. With interactions, competition between interaction and random forces causes transport to first increase then decrease with temperature. Alterations in the bottleneck and periodicity of the corrugated channel also contribute to the transition between the absence of transport and a finite net transport. Ultimately, the average velocity diminishes as the coupling strength and characteristic length increase. Our findings show that there exist competitions among the bottleneck and the periodicity, the interaction (i.e., the coupling strength and characteristic length), temperature, and driving force. In particular, the ranges of parameters determine the state of transports (e.g., no transport or a finite net transport). For example, the transport disappears when the characteristic length is larger than the bottleneck and arises when the characteristic length is smaller than the bottleneck. Our results may narrow the gap between the transport with the hydrodynamic memory in theory and that in experiment.

In this study, our selection of the Lennard–Jones potential was motivated by its basis in established experimental work.[12,55] Therefore, our discussion has been restricted to particles interacting via the Lennard–Jones potential; it did not encompass other interaction types mentioned in the introduction.

The findings are obtained through the analysis of time series, the probability distribution of positions over various intervals, and phase space examination. These analyses reveal underlying physical mechanisms (e.g., the clogging, collective motion, and independent directional motion) responsible for the observed transport phenomena. Our study offers a comprehensive investigation into the influence of system parameters on this transition. The exploration of such a transition is characteristic of an ideal sensor. Based on experiments mentioned above, the functionality of our proposed sensor may be experimentally achievable through microfluidic assays. Our results have potential applications for research on managing transport with hydrodynamic memory in biology, physics, chemistry, and beyond.

Appendix A

To understand the dynamical relaxation of the interacting particles, we show the mean square displacement with different auxiliary particles, the mobility depending on the initial condition, the average velocity for different g_n in Figs. A1–A3.

Without the corrugated channel, the interaction and driving force, figure A1 shows the mean square displacement with different auxiliary particles. For $T = 0.001$, figure A1(a) displays that the diffusion without auxiliary particle or a few auxiliary particle (e.g., $M = 3$) is ballistic. For $M = 8$, the power-law exponent α of the mean square displacement is 1.765. Notice that the power-law exponent α corresponding to $M = 13$ is 1.5, which is equal to that presented in the equation. Moreover, it is shown that the power-law exponent α of the mean square displacement corresponding to $M = 15$ is identical to that corresponding to $M = 13$. For $T = 0.1$, the power-law exponents α corresponding to $M = 0$, 3, and 8 do not match $\alpha = 3/2$ in equation. While the power-law exponents α corresponding to $M = 13$ and 15 are identical to $\alpha = 3/2$ in equation. Therefore, the number of auxiliary particles ensure that the diffusion of the particles match the power-law exponent α in the equation of numerical simulation.

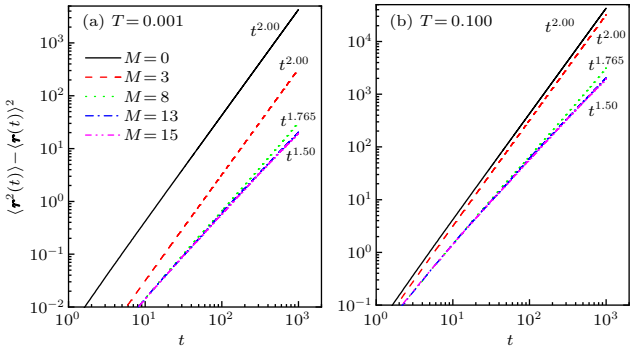


Fig. A1. Without the corrugated channel, the interaction, and driving force, the mean square displacement with different auxiliary particles M for $T = 0.001$ (a) and $T = 0.1$ (b) . The other parameters are $\alpha = 3/2$, $m = 1.0$, $\mu_0 = 1000$, $b = 5$.

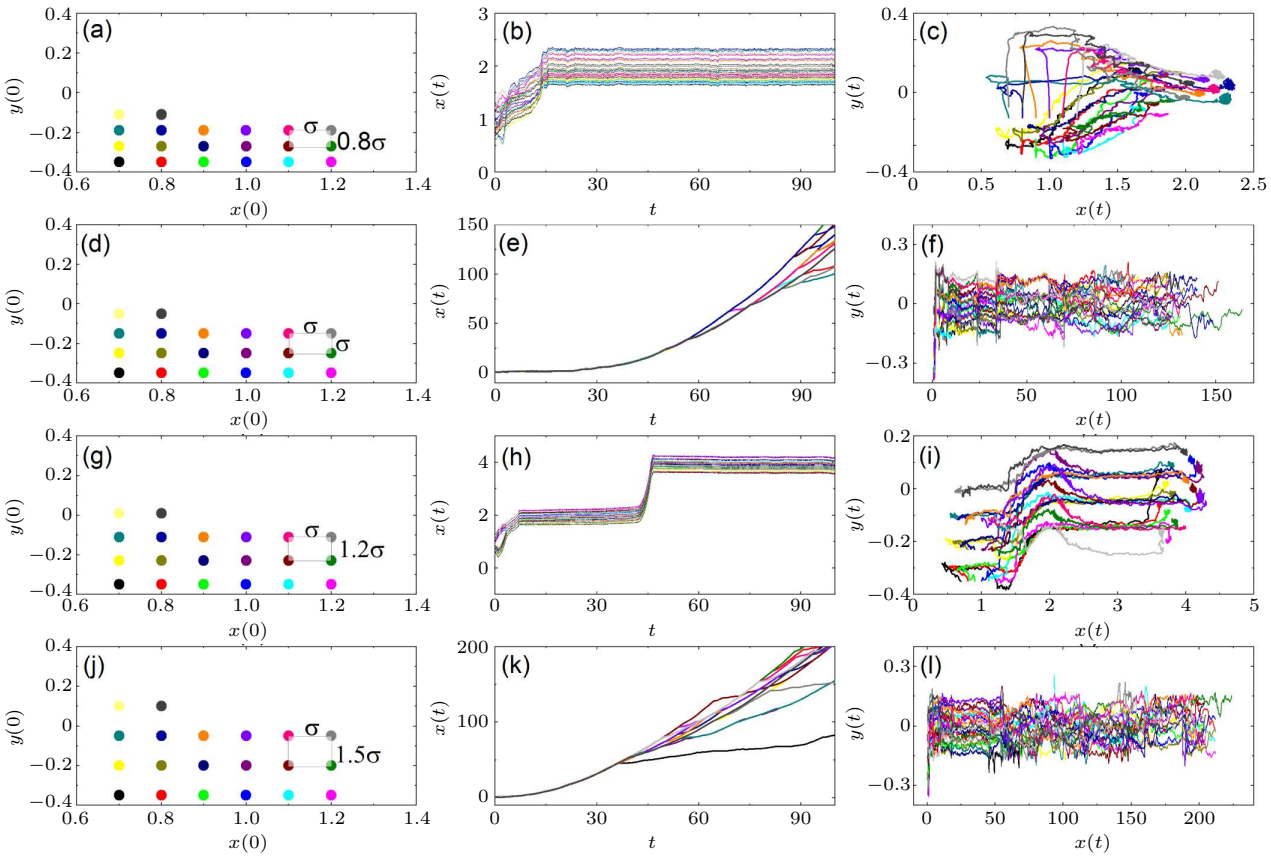


Fig. A2. The time series $x(t)$ of interacting particles (the second column) and phase space maps (the third column) for different initial positions (the first column). The other parameters are $\alpha = 3/2$, $m = 1.0$, $\mu_0 = 1000$, $b = 5$, $F = 0.5$, $T = 0.01$, $\epsilon = 0.5$, $\sigma = 0.1$, and $L = 2.0$.

To interpret the transport depending on the initial conditions, we plot the the time series $x(t)$ of interacting particles and phase space maps in Fig. A2(a) for different initial conditions. Figure A2(a) shows the initial positions of 20 interacting particles. The distances of x and y directions are σ and 0.8σ, respectively. Figure A2(b) shows the time series x of 20 interacting particles, which displays that all particles trivially move in the x direction first, and then trivially oscillate at equilibrium positions in the first bottleneck. To obtain more insight in this behavior, we plot its phase space map in Fig. A2(c), showing that after short relaxation, all particles oscillate at their equilibrium positions. This is a solid-like state.

Figure A2(d) shows the initial positions of 20 interacting particles which the distances of x and y directions are both σ. The time series x of interacting particles are plotted in Fig. A2(e), showing that there is a curve before $t = 60$. This suggests the appearance of collective motion. Then as time evolution, the curves become more and more, implying that the collective motion disappears. This state is the liquid-like state. The more details are shown in Fig. A2(f).

Figure A2(g) shows the initial positions of 20 interacting particles which the distances of x and y directions are σ and 1.2σ, respectively. We find from Fig. A2(h) that all particles move through the first period and oscillate at equilibrium positions in second bottleneck. The more details are shown in Fig. A2(i). Figure A2(j) shows the initial positions of 20 interacting particles which the distances of x and y directions are σ and 1.5σ, respectively. The behaviors of Figs. A2(k) and A2(l) are similar to those of Figs. A2(h) and A2(i), respectively. In summary, the motions of interacting particles sensitivity depend on the initial conditions.

Figure A3 shows the average velocities $\langle v \rangle$ as a function of temperature T. For a large bottleneck (e.g., $g_n = 0.3$ and 0.5), $\langle v \rangle$ decreases with the increase of T. However, for a small bottleneck (i.e., $g_n = 0.1$), there coexist a maximum and a minimum of $\langle v \rangle$ with the increase of T in the insets. It is clear that as temperature increases, the average velocity decreases first, then increases and decreases finally. Compared to the average velocity for different g_n, it is clear that the average velocity corresponding to $g_n = 0.5$ is larger than that corresponding to $g_n = 0.3$. Namely, the large the bottleneck is, the large $\langle v \rangle$ is.

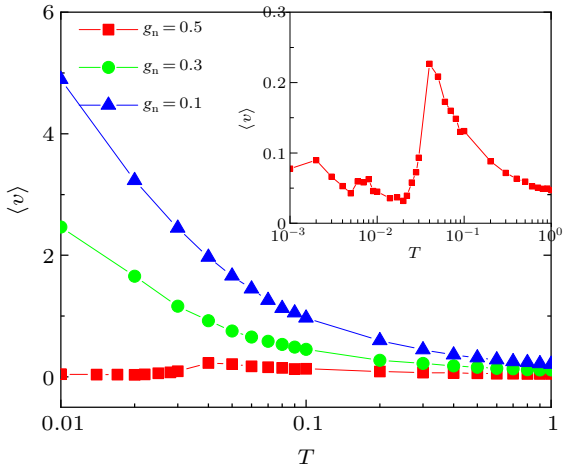


Fig. A3. The average velocity as a function of the temperature. The insets show the dependence of the average velocity on temperature for $g_n = 0.1$. The other parameters are $\varepsilon = 0.5$, $\sigma = 0.1$, $F = 0.5$, $N = 20$, and $L = 2.0$.

Acknowledgments

Project supported by the National Natural Science Foundation of China (Grant Nos. 12365007 and 12265017), Yunnan Fundamental Research Projects (Grant Nos. 202101AS070018 and 202101AV070015), the Scientific Research Foundation of the Yunnan Provincial Department of Education (Grant No. 2023J1208), Xingdian Talents Support Program, and Yunnan Province Ten Thousand Talents Plan Young & Elite Talents Project, and Yunnan Province Computational Physics and Applied Science and Technology Innovation Team. The numerical simulation and significance estimation were performed on the Key Laboratory of High-Density Computing, Zhaotong University.

References

[1] Reguera D, Schmid G, Burada P S, Rubí J M, Reimann P and Hänggi P 2006 *Phys. Rev. Lett.* **96** 130603
[2] Wang Y T, Sun X L, Luo L Y, Zhang Z M, Li H P, Jiang D J and Zhou M S 2023 *Chin. Phys. B* **32** 095201
[3] Gao Z Y, Dong W, Tian C B, Jiang X Z, Dai Z L and Song Y H 2024 *Chin. Phys. B* **33** 095203
[4] Jing P, Haque F, Shu D, Montemagno C and Guo P 2010 *Nano Lett.* **10** 3620
[5] Braun A, Varga-Szabo D, Kleinschnitz C, Pleines I, Bender M, Austinat M, Bosl M, Stoll G and Nieswandt B 2009 *Blood* **113** 2056
[6] Reguera D, Luque A, Burada P S, Schmid G, Rubí J M and Hänggi P 2012 *Phys. Rev. Lett.* **108** 020604
[7] Ghosh P K, Hänggi P, Marchesoni F, Nori F and Schmid G 2012 *Europhys. Lett.* **98** 50002
[8] Malgaretti P, Pagonabarraga I and Rubi J M 2014 *Phys. Rev. Lett.* **113** 128301
[9] Li Y, Ghosh P K, Marchesoni F and Li B 2014 *Phys. Rev. E* **90** 062301
[10] Ao X, Ghosh P K, Li Y, Schmid G, Hänggi P and Marchesoni F 2014 *Eur. Phys. J. Spec. Top.* **223** 3227
[11] Bayley H and Cremer P S 2001 *Nature* **413** 226
[12] Yang X, Liu C, Li Y, Marchesoni F, Hänggi P and Zhang H P 2017 *Proc. Natl. Acad. Sci. USA* **114** 9564
[13] Hoyles M, Kuyucak S and Chung S H 1998 *Phys. Rev. E* **58** 3654
[14] Di Carlo D 2009 *Lab Chip* **9** 3038
[15] Guerin T, Levernier N, Benichou O and Voituriez R 2016 *Nature* **534** 356
[16] Haque F, Geng J, Montemagno C and Guo P 2013 *Nat. Protoc.* **8** 373
[17] Herisson F, Frodermann V, Courties G, Rohde D, Sun Y, Vandoorne K, Wojtkiewicz G R, Masson G S, Vinegoni C, Kim J, *et al.* 2018 *Nat. Neurosci.* **21** 1209
[18] Pardo-Pastor C, Rubio-Moscardo F, Vogel-Gonzalez M, Serra S A, Afthinos A, Mrkonjic S, Destaing O, Abenza J F, Fernandez-Fernandez J M, Trepat X, *et al.* 2018 *Proc. Natl. Acad. Sci. USA* **115** 1925
[19] Bi G, Su M, Li N, Liang Y, Dang S, Xu J, Hu M, Wang J, Zou M, Deng Y, *et al.* 2021 *Cell* **184** 3528
[20] Kefauver J M, Ward A B and Patapoutian A 2020 *Nature* **587** 567
[21] Benichou O and Voituriez R 2008 *Phys. Rev. Lett.* **100** 168105
[22] Souzy M, Allard A, Louf J F m c, Contino M, Tuval I and Polin M 2022 *Phys. Rev. Res.* **4** L022029
[23] Robins T, Camacho J, Agudo O C, Herraiz J L and Guasch L 2021 *Sensors* **21** 4570
[24] Goychuk I and Kharchenko V 2012 *Phys. Rev. E* **85** 051131
[25] Kharchenko V O and Goychuk I 2013 *Phys. Rev. E* **87** 052119
[26] Goychuk I and Poschel T 2020 *Phys. Rev. E* **102** 012139
[27] Goychuk I 2019 *Biosystems* **177** 56
[28] Goychuk I 2015 *Phys. Rev. E* **92** 042711
[29] Mei R, Xu Y and Kurths J 2019 *Phys. Rev. E* **100** 022114
[30] Burov S and Barkai E 2008 *Phys. Rev. Lett.* **100** 070601
[31] Siegle P, Goychuk I and Hänggi P 2010 *Phys. Rev. Lett.* **105** 100602
[32] Franosch T, Grimm M, Belushkin M, Mor F M, Foffi G, Forró L and Jeney S 2011 *Nature* **478** 85
[33] Goychuk I 2019 *Phys. Rev. Lett.* **123** 180603
[34] Henry B I, Langlands T A M and Wearne S L 2008 *Phys. Rev. Lett.* **100** 128103
[35] Alkahtani B S T 2016 *Chaos Soliton. Fract.* **89** 547
[36] Chen S B, Jahanshahi H, Abba O A, Solís-Pérez J E, Bekiros S, Gómez-Aguilar J, Yousefpour A and Chu Y M 2020 *Chaos Solitons Fractals* **140** 110223

[37] Knapp C, Chew A and Alicea J 2020 *Phys. Rev. Lett.* **125** 207002
[38] Zhang Y, Liu X, Belić M R, Zhong W, Zhang Y and Xiao M 2015 *Phys. Rev. Lett.* **115** 180403
[39] Moreira A A, Vieira C M, Carmona H A, Andrade J S and Tsallis C 2018 *Phys. Rev. E* **98** 032138
[40] Guerreiro T, Martin A, Sanguinetti B, Pelc J S, Langrock C, Fejer M M, Gisin N, Zbinden H, Sangouard N and Thew R T 2014 *Phys. Rev. Lett.* **113** 173601
[41] Tateno M, Yanagishima T, Russo J and Tanaka H 2019 *Phys. Rev. Lett.* **123** 258002
[42] Park S C 2020 *Phys. Rev. E* **102** 042112
[43] Lind T K, Zielińska P, Wacklin H P, Urbańczyk-Lipkowska Z and Cárdenas M 2014 *ACS Nano* **8** 396
[44] Thomas C C and Durian D J 2015 *Phys. Rev. Lett.* **114** 178001
[45] Thomas C C and Durian D J 2016 *Phys. Rev. E* **94** 022901
[46] Chieco A T, Zu M, Liu A J, Xu N and Durian D J 2018 *Phys. Rev. E* **98** 042606
[47] Majmudar T S, Sperl M, Luding S and Behringer R P 2007 *Phys. Rev. Lett.* **98** 058001
[48] Wang W, Cherstvy A G, Kantz H, Metzler R and Sokolov I M 2021 *Phys. Rev. E* **104** 024105
[49] Kursawe J, Schulz J and Metzler R 2013 *Phys. Rev. E* **88** 062124
[50] Siegle P, Goychuk I and Hänggi P 2011 *Europhys. Lett.* **93** 20002
[51] Vojta T, Halladay S, Skinner S, Janusonis S, Guggenberger T and Metzler R 2020 *Phys. Rev. E* **102** 032108
[52] Geiger M, Spigler S, d'Ascoli S, Sagun L, Baity-Jesi M, Biroli G and Wyart M 2019 *Phys. Rev. E* **100** 012115
[53] Mongera A, Rowghanian P, Gustafson H J, Shelton E, Kealhofer D A, Carn E K, Serwane F, Lucio A A, Giammona J and Campàs O 2018 *Nature* **561** 401
[54] Hentschel H G E, Procaccia I and Roy S 2019 *Phys. Rev. E* **100** 042902
[55] Zhu Q, Zhou Y, Marchesoni F and Zhang H P 2022 *Phys. Rev. Lett.* **129** 098001